Microscopic evidence for phase separation of organic species and inorganic salts in fine ambient aerosol particles

Li, Weijun; Liu, Lei; Zhang, Jian; Xu, Liang; Wang, Yuanyuan; Sun, Yele; Shi, Zongbo

Document Version
Peer reviewed version

[Link to publication on Research at Birmingham portal](#)

Microscopic evidence for phase separation of organic species and inorganic salts in fine ambient aerosol particles

Weijun Li[1*], Lei Liu[1], Jian Zhang[1], Liang Xu[1], Yuanyuan Wang[1], Yele Sun[2], Zongbo Shi[3*]

[1]Department of Atmospheric Sciences, School of Earth Sciences, Zhejiang University, 310027, Hangzhou, China

[2]State Key of Laboratory of Atmospheric Boundary Physics and Atmospheric Chemistry, Institute of Atmospheric Physics, Chinese Academy of Sciences, Beijing 100029, China

[3]School of Geography, Earth and Environmental Sciences, University of Birmingham, UK

Correspondence to: Weijun Li (liweijun@zju.edu.cn); Zongbo Shi (z.shi@bham.ac.uk)

Abstract Phase separation is an important microscopic phenomenon in aerosol particles and reflects the surface properties of particles and the aging degree of organic components. However, few data are available to directly reveal phase separation in ambient aerosol particles, although there are abundant data from laboratory experiments. In this study, different state-of-the-art microscopic technologies were used to study phase-separation of organic matter (OM) and inorganic salts in individual particles collected from different atmospheric environments, with one type of surrogate particles prepared in laboratory. We found that most of the collected particles with an equivalent sphere diameter > 100 nm have a secondary inorganic aerosol core with OM coating in the continental atmosphere. In addition, secondary inorganic aerosol and OM phase separation is more frequent in rural particles than suburban particles, suggesting that particle aging enhances phase separation. Our results show that phase separation is a frequent phenomenon that forms organic coatings on inorganic particles of individual particles (> 100 nm) and their number abundances depend on the particle size and OM aging degree. The resulting morphology shows that OM is an important particle surface in the atmosphere, which influences gas partitioning, optical and hygroscopic properties, and cloud condensation nuclei formation activities.

1. Introduction

Atmospheric aerosol particles have strong effects on the climate and public health. Organic matter (OM) and secondary inorganic aerosols are the two dominant components of aerosol particles, which account for over 50% of the total PM2.5 mass in both urban and nonurban areas.[1, 2] Many studies have found that both organic compounds and sulfuric acid are involved in particle formation and growth from the nucleation to the accumulation modes,[3-6] indicating that they are internally mixed in many of the individual aerosol particles.[7] Because of the complex formation mechanism and oxidation of OM in size-resolved atmospheric particles, organic aerosols might display different mixing properties with secondary inorganic aerosols,[8, 9] which determines their hygroscopicity, cloud condensation nuclei (CCN) activity, and optical properties.[10-13] It may also affect the formation rates of organic and inorganic aerosols.[3, 14, 15] For example, Zhang et al.[16] showed that the alpha-pinene SOA coating on an inorganic sulfate particle significantly reduced the reactive uptake of isoprene-derived epoxydiols (IEPOX).

Recently, You et al.[17] inferred that liquid-liquid phase separation can separate secondary organic matter (SOM) and sulfate into individual particles. The formation of a SOM coating on an inorganic aerosol core has been frequently detected in ambient particles by transmission and scanning electron microscopy.[18-21] Time-of-flight secondary ion mass spectrometry (TOF-SIMS) and X-ray Absorption Near Edge Structure spectra (XANES) were also used to determine organic species of the SOM coating, such as shorter chain or more oxygenated groups, including carboxylic acids,

alkyl groups, and oxygen bonded alkyl groups.[19, 22, 23] The SOM coating of amorphous semisolid phases can decrease the uptake of reactive trace gases on particles due to its high viscosity and low diffusion coefficient of organic substances based on the laboratory experiment and global observation/modelling simulation.[17, 24] Recently, the IEPOX-derived organosulfate formations have been shown to create a shell with an inorganic sulfate core.[16, 25] Although OM within individual particles is constantly modified by interactions with gas-phase oxidants and radicals, as well as with atmospheric water vapor, the hygroscopicity of the particle and its optical properties will differ substantially depending on whether the OM is on the surface or in the interior.[26] Laboratory experiments indicate that the mixing structures of OM and secondary inorganic aerosols could exhibit a core-shell, partially engulfed configurations, or a homogeneous mixture depending on the O/C ratio, organic-to-inorganic ratio, RH,[27, 28] and particle size.[29-31] Phase separation normally occurs when the relative humidity is below the separation relative humidity (SRH),[17] indicating that humidity is very important for the phase separation characteristics of particles.[32] If phase separation is observed in a particle, the core and the outer layer are morphologically separated, and organic and inorganic species are present in individual particles. In the laboratory experiments, the complex mixtures of some surrogate OMs were used for a mixing simulation with sulfate,[33] whereas individual ambient organic aerosols can contain complex oxidized OM from a wide range of volatile organic compounds in the real atmosphere.[3, 8] To date, the majority of studies on the aerosol phase separation phenomenon and its thermodynamics have been carried out on

76 surrogates in the laboratory[34-36]; however, very few studies observed phase separation

77 of atmospheric particles.[37-39] Here, we focus on phase separation of fine particles (≤ 2.5

78 μm) in the ambient air. Therefore, it is necessary to observe the mixing structure of

79 organic aerosols collected in ambient air, instead of the defined aerosols and size ranges

80 that are typical of laboratory experiments.

81

82 **2. Experimental Methods**

83   Aerosol samples were collected during the international field campaigns including

84 the Air Quality Research in Beijing and the surrounding region in 2013, and the winter

85 haze in the North China Plain during 2015. Twenty-three aerosol samples were

86 collected at the suburban Xianghe site in Beijing (39.798° N, 116.958° E) and at the

87 rural Yucheng site in Jinan (36.95°N, 116.60° E) from June 11–30, 2013, and ultrafine

88 particles were collected at an urban site in Jinan (36.68° N, 117.06° E) during two haze

89 days and one clean day from January 11-23, 2016. All of the sampling information is

90 listed in Table S1. The Xianghe site is in a suburban area approximately 50 km southeast

91 of downtown Beijing and 85 km northwest of downtown Tianjin. During the sampling

92 period, this site experienced frequent mixed plumes from urban activities, industries,

93 and agricultural biomass burning. The rural Yucheng site is subject to the influences

94 from long-range transported pollutants, especially from agricultural biomass burning.

95 The urban site in Jinan consists of densely populated residential areas, urban streets,

96 and light industry. The oxygen-to-carbon (O/C) ratio of organic matter (OM) and the

97 organic-to-inorganic ratio in submicron aerosols at the Xianghe site were determined

98   from collecting measurements with an Aerodyne aerosol chemical speciation monitor

99   (ACSM) during the sampling period (Table S3).[40]

100   Aerosol particles were collected onto copper TEM grids coated with carbon film

101   or lacey carbon TEM grids (carbon type-B, 300-mesh copper, Tianld Co., China) by a

102   single-stage cascade impactor with a 0.5 mm diameter jet nozzle and an air flow rate of

103   1.0 l min^{-1}. This sampler has a collection efficiency of 50% at a 260 nm aerodynamic

104   diameter, assuming the density of the particle is 2 g cm^{-3}. To collect ultrafine particles,

105   we developed a new single-stage cascade impactor with a 0.3 mm diameter jet nozzle.

106   Aerosol particles are pre-filtrated through the 100 nm pore size of a polycarbonate

107   filters, which means the impactor can only collect particles less than 100 nm in size at

108   an air flow rate of 5l min^{-1}. The lacey carbon and carbon-film TEM grids were both

109   used as substrates to collect the ultrafine particles. Aerosol samples were collected on

110   clear and haze days, with relative humidity ranging from 40% to 75%. After particle

111   collection, each sample was placed in a sealed dry plastic tube and stored in a desiccator

112   at 25ºC and 20 ± 3% RH to minimize the exposure to ambient air and preserve the

113   sample for analysis. Moreover, we made one type of surrogate particles, which

114   consisted of NaCl coated with an organic coating in the laboratory experiments. First,

115   we sprayed micrometer NaCl particles from the NaCl solution onto the TEM grid, and

116   then, we put the sample into a photochemical reaction chamber, which can produce the

117   oxidized organic matter (Figure S1). We left the TEM grid in the chamber for

118   approximately 20 hours and found that the oxidized organic species condensed on the

119   grid and formed one organic coating on the NaCl particles. The details of the

120   environmental chamber and sample preparations used in this study can be referenced

121   in Zhang et al. (2020).[41]

122   The composition and morphology of individual particles collected in different

123   environmental conditions and prepared in the laboratory were analyzed with a JEOL

124   JEM-2100 TEM operated at 200 kV and coupled with X-ray energy diffraction

125   (TEM/EDS). In our study, the effects of water and semi-volatile organics were not

126   considered. The pure NH_4NO_3 particles on the filters can be observed in TEM (Figure

127   S2). The details of the laboratory experiment are described in a previous study.[41] To

128   better observe residual OM mixed with ultrafine particles, TEM was utilized to observe

129   ultrafine particles adhering to the lacey carbon, and sulfate particles were compared

130   before and after the sublimed process under the electron beam. To minimize beam

131   damage, we used a weak electron beam for the TEM observations. No obvious change

132   in the morphology and mixing structure of individual particles was observed (see

133   further explanation in section 3).

134   Imaging particles with cryo-TEM was conducted on a Talos F200C equipped with

135   a Ceta 4k × 4k camera at the Center of Cryo-Electron Microscopy at Zhejiang

136   University (Hangzhou, China), which was operated at a 200 kV accelerating voltage.

137   Samples were cooled in the cryo-TEM to approximately 104 K using a liquid nitrogen-

138   cooled cryo-TEM holder before exposure to electron radiation to reduce damage to the

139   particles. The cryo-TEM is the best way to observe the original condition of individual

140   secondary particles on the substrate before the secondary nitrates or sulfates are

141   damaged under electron beam. In this study, we analyzed 302 particles in three samples

142   using the cryo-TEM to confirm the core-shell structure (Table S1).

143   For statistical analysis, the equivalent circle diameters (ECDs) of individual

144   particles were determined by the iTEM software (Olympus soft imaging solutions

145   GmbH, Germany). In addition, atomic force microscopy (AFM) was used to determine

146   the equivalent spherical diameter (ESD) of individual particles on the substrate. The

147   relationship of the ECD to the ESD were evaluated. In this study, we calculated the

148   ESD based on the equations in the supplemental materials. To quantify the thickness of

149   the OM coating, the ESDs of individual particles and inorganic aerosol cores were

150   measured in the TEM images and the AFM.

151   After the TEM observations, four typical samples collected at the Xianghe (two

152   samples) and Yucheng sites (two samples) were selected for hygroscopic experiments

153   in the laboratory. Phase changes of the surrogate samples were also observed under

154   different relative humidity (RH). An individual particle hygroscopicity (IPH) system

155   was employed to observe the hygroscopic properties of individual particles at RH

156   values from 3% to 94%. The experimental process includes (1) introducing N_2 gas with

157   controlled flow by a mass flow controller into a chamber; (2) mounting the TEM grid

158   or silicon wafer with particles on the bottom of an environmental microscopic cell

159   (Gen-RH Mcell, UK), which can change the RH and maintain a constant temperature

160   of 20 °C; and (3) taking images at different RH through an optical microscope (Olympus

161   BX51M, Japan) with a camera (Canon 650D). The growth factor of individual particles

162   was determined by calculating the diameter of particles during hydration and its dry

163   diameter. The quantification standard of the individual particle hygroscopic system and

the growth factor calculation have been introduced by Sun et al. [32] This analysis also provides deliquescence and efflorescence relative humidity of the individual particles at 20°C.

Typical samples at suburban and rural sites were analyzed using a nano-scale secondary ion mass spectrometer (NanoSIMS 50, CAMECA Instruments, Geneviers, France). A micro-cesium source was used to generate Cs^+ primary ions, with an impact energy of 16 kV for sample interrogation, and was used to the analyze samples for $^{12}C^-$, $^{16}O^-$, $^{12}C^{14}N^-$, and $^{32}S^-$ ions. We recognize that the quality of the $^{12}C^-$ intensity map was affected by the carbon substrate in the TEM grid. Although the $^{12}C^-$ and $^{12}C^{14}N^-$ intensity maps display the same distribution in the samples (Figure S4), $^{12}C^{14}N^-$ is adopted to represent organic matter in individual particles and $^{32}S^-$ can indicate secondary sulfates.[37, 42] This coupling of NanoSIMS with TEM analysis can precisely determine the mixing properties of organic and inorganic aerosols in individual particles (Figure 4).

We also calculated the hygroscopicity parameter, Kappa (κ) value, through the Zdanovskii, Sotes, and Robinson (ZSR) assumption by using the measured data of individual internally and externally mixed particles[43]. The calculation method is introduced in the supplemental materials.

3. Results and Discussion

Figure 1 displays the phase separation of surrogate particles (NaCl: dark/grey + OM: yellow) prepared in the laboratory under different RHs. The NaCl cores changed

from solid to liquid at a RH between 75% to 90% during hydration or from liquid to

solid at a RH between 55% to 20% RH during dehydration, and the organic coatings

consistently separated from NaCl in the individual particles (Figure 1). This indicates

that phase separation between organic and inorganic components continuously occurs

in individual particles as the RH increases. We further used the TEM/EDS to confirm

the organic coating and the NaCl core in surrogate particles. Figure 2 shows that

individual particles kept the stable phase separations in the high vacuum chamber of

the TEM. Therefore, the laboratory experiments show that individual particles from the

solid to liquid phase under different RHs can consistently keep the organic-inorganic

phase separation before the SRH is reached.

To examine how beam damage might affect the phase separation and core/shell

ratio, we observed the morphology of 302 particles from three randomly selected

samples in a cryo-TEM. In the low temperature TEM chamber, beam damage to

particles is minimized. However, we did observe some "white dots" in core (Figures

3b-f) and "blank parts" between core and coating (Figures 3b, c, g). Our laboratory

analysis on standard samples suggest that the white dots may be caused by the

evaporation of semi-volatile compounds during the sample storage (Figure S2). The

"blank parts" in core-shell particles have been widely observed in ambient particles.[20,]

[21] This is likely due to the crystallization of sulfates in the aerosol particles but not for

the OM coating during drying, leading to a different degree of shrinking. Figures 3a-f

show that these particles all maintained their original particle morphology on the

substrate, i.e., there was no obvious sublimation of nitrate/sulfate particles.

208   The cryo-TEM measurement provides direct evidence that many particles collected

209   in different atmospheric environments display a typical core-shell structure (Figure 3).

210   The high magnification of cryo-TEM images clearly shows particles on the substrate

211   without obvious beam damage, with evidence of organic coatings on the inorganic

212   aerosols (Figures 3b-g). If the particles are exposed to the electron beam for a long time

213   (>15 seconds), we started to observe particle damage in the inorganic cores, but not in

214   the organic coatings. For example, Figure S3 presents the original particle and the

215   slightly sublimed particle under the electron beam. This confirms that the beam damage

216   did not change the thickness of organic coatings and particle size in individual particles.

217   Figures 4a-e further show that there is no obvious beam damage in the TEM images.

218   Therefore, the data collected from the regular TEM generally reflects the morphology

219   and mixing structure of individual particles.

220   The state-of-the-art NanoSIMS technique provides more conclusive evidence on

221   the distribution of organic and inorganic components in individual particles.[37, 39] In this

222   study, the NanoSIMS confirmed that the coating as OM, illustrated by the $^{12}C^{14}N^-$ signal

223   from the ambient aerosol particles (Figure 4g and Figures S4-5). Combined with the

224   cryo-TEM observation, as shown in Figures 3 and 4a-c, the strong $^{32}S^-$ signal in the

225   core and detected by the NanoSIMS (Figure 4h) comes from inorganic sulfate and/or

226   sulfide. Additionally, the OM-coated particles (Figures 3 and Figures 4a-c), OM-

227   disperse (Figure S6a), dumbbell (Figures S6b-c), and homogeneous structure (Figures

228   4d-e) were also observed in the samples. The details regarding particle classifications

229   have been described by Li et al.[7] In this study, no clear OM-coating was observed for

230   the nanometer (< 100 nm) secondary aerosol particles, except for the dumbbell structure

231   of OM and inorganic aerosols (Figure S6c). This is further confirmed in the NanoSIMS

232   analysis, as shown in the ion intensity threshold maps (Figures 4g-h and Figure S5).

233   Compared with the ultrafine inorganic particles that were observed before and after the

234   subliming process under electron beam (Figures 4e-f), TEM clearly detected residual

235   OM left by the sublimed inorganic particles. We also investigated phase separation in

236   two types of laboratory generated particles (i.e. ammonium sulfate and mixture of

237   ammonium sulfate/oxalate, Figure S7). It shows the residual OM on the substrate after

238   the sublimation of inorganic components from the ammonium sulfate and oxalate

239   mixture but not pure ammonium sulfate particle. Moreover, the NanoSIMS analysis

240   indicates that the OM likely homogeneously mixed with ultrafine sulfate particles (e.g.,

241   particles A, B, and C in Figure 4g).

242   The high magnification TEM images not only display the OM coating on inorganic

243   particles, but also show its thickness (Figures 3 and 4). At the suburban site, 34% of

244   particles display OM-coating structure at the size range from 100 nm to 2 μm (Figures

245   5a, c and Figure S8). The fraction of inorganic particles with OM coating at the rural

246   site is as high as 55% (Figures 5b, d and Figure S8). Based on the size measurements

247   of AFM and TEM, we calculated the mean thickness of OM coating, which is 70 nm at

248   the suburban site and 120 nm at the rural site (Figure 5 and Figure S9). Figure 5 shows

249   the percentage of individual particles with phase separation between inorganic aerosols;

250   it also illustrates and that the thickness of OM coating increases as the size increases

251   from 100 nm to 500 nm. Moreover, we noticed that the NO/NO_x ratio was at 0.30±0.23

at the suburban site, but only 0.04±0.05 at the rural site during the sampling period, suggesting that the rural air masses are more aged than the suburban air masses (Table S2 and Figure S10). Based on the microscopic measurements (Figures 3 and 5), we found that more secondary inorganic particles tend to have OM coatings, whose thickness increases as the particles are aging from the urban to rural air. However, our data show that phase separation of OM and inorganic aerosols is a widespread phenomenon in all environments. It should be noted that a significant fraction of inorganic aerosols and OM mixture particles do not undergo phase separation in the atmosphere (Figure 5).

The O/C ratios in organic aerosols have been shown to assist in determining the phase separation in organic and inorganic mixtures.[12, 33] We calculated the O/C ratio of aerosol particles at the suburban site, which ranges from 0.36 to 0.60, with an average of 0.49; The OM to sulfate ratio ranges from 1 to 4.5, with an average of 1.7 in the ambient aerosols (Table S3). At the rural site in the North China Plain, the average O/C ratio is up to 0.6.[44, 45] Therefore, the O/C ratio from bulk fine aerosols collected in the North China Plain is lower than the value of 0.8 for phase separation[33] and is also lower than that (0.92) reported by Ott et al. [46] The O/C ratio of < 0.8 in OM explains why OM-coated structure particles are the most abundant aerosols at the rural site in this study.[17] It should be noted that there are still certain fractions of individual particles > 100 nm with a homogeneous mixing structure of OM and inorganic aerosols (Figure 4d and Figure 5). The reason for this could be attributed to an O/C ratio of > 0.8 in secondary organic aerosols, which underwent more aging processes in the atmosphere.

The fraction of particles with phase separation of OM and inorganic aerosols gradually reduces to less than 5% from 2 μm to 100 nm (Figures 3 and 5c-d). In particular, we could not find a clear OM coating in most of the particles that were smaller than 100 nm (e.g., Figures 4e-f), although there are a few dumbbell structures between inorganic aerosols and OM (e.g., Figure S6b). This phenomenon is similar to a laboratory experiment showing that OM and inorganic aerosols in ultrafine particles can become engulfed structure (i.e., dumbbell in this study).[29, 47] A recent laboratory experiment proposed that phase separation can completely disappear at the smallest particle size down to 48 nm.[48] Moreover, Cheng et al.[31] suggested that atmospheric secondary organic particles at room temperature are expected to always be liquid at diameters below ~20 nm. Here, we could not exactly determine whether there is an OM coating on inorganic aerosols in the ultrafine particles (<100 nm), based on the TEM observations. One reason is that it is difficult to identify the OM film using TEM observation if it is extremely thin (Figure 4e); and the second reason is that the drying speed on the substrate might influence phase separation in the ultrafine particles.[30] Although our study could not precisely determine phase separation in ultrafine particles, as done by the previous laboratory experiments,[29, 48] we found an increase in the fraction of particles with phase separation with particle size (Figure 5). This suggests that particle size could be an important factor affecting the core-shell mixing structure of OM and inorganic aerosols, in addition to the O/C and organic-to-inorganic ratios.[12, 27]

To understand how organic coatings influence atmospheric properties of inorganic aerosols, a series of laboratory experiments and theory calculations were further

conducted in this study. Hygroscopic experiments were completed for atmospheric particles using an individual particle hygroscopic system. We determined the average ERH value as ~33% and DRH as ~80% (Figures S11 and S12). This is in reasonable agreement with the DRH and ERH values predicted from the model developed by Bertram et al.[12] using the ACSM data (O/C and organic/sulfate ratio) (Table S3). We further calculated the SRH values at a range of 74% to 97% with an average value at 88% (Table S3). By comparing the SRH and DRH values in Table S3, we suggest that these OM-coating particles observed on the substrate should keep the phase separation in the ambient air. In other words, these OM-coated particles should be phase separated (i.e., OM coating and inorganic core) in the ambient air during the daytime (RH at 11% to 80%) in the North China Plain.

In this study, many studies suggest that OM coating on inorganic particles is secondary to organic aerosols.[7, 17, 19, 22] In the laboratory, our hygroscopic experiments of individual aerosol particles showed that the OM coatings caused the deliquescence of particle surfaces at a RH lower than 63% to 66% (Figures S11 and S12), which agrees with a previous study on the mixture of particles between secondary OM and inorganic salts generated in the laboratory.[41, 49] OM coatings can also reduce water uptake and inhibit the water uptake of inorganic salts following a RH increase.[11] On the other hand, once these internally mixed particles become aqueous droplets, the OM coating can inhibit the water evaporation in the aerosol.[50]

In this study, we further calculated the κ of individual particles containing OM coatings and ammonium sulfate cores based on size data from the TEM measurement,

15

as shown in Figure 5. We estimate $\kappa=0.37$ for OM-inorganic core-shell particles at the suburban site and $\kappa=0.30$ at the rural site (Figure S13). The result indicates that the thicker coatings in core-shell particles (>100 nm) at the rural site than at the suburban site (Figure 5) decreased the κ value. The calculated theoretical result is similar to the measured values ($\kappa= 0.3\pm0.1$) using a Droplet Measurement Technology continuous flow CCN counter in the North China Plain.[51] In addition, we identified that the mean κ of individual particles increases following particle size (> 100 nm) increase (Figure S14). This is attributed to more inorganic species that are contributing to particle growth than organic species in the core-shell secondary particles. Organic coatings on the nanoparticles might have a different influence on κ values than that of large particles.

4. Summary and Atmospheric implications

The phase separation of OM and inorganic aerosols has been extensively studied in the laboratory because mixing structures of OM and inorganic aerosols in individual particles can determine their optical property, gas partitioning, heterogeneous reactivity, hygroscopic property, and CCN ability.[10-13] Laboratory experiments have showed that mixing structures of OM and sulfate with diameters in submicronmeters depend on particle size and O:C values in OM.[29] However, there are only few studies to confirm the phase separation in fine aerosol particles (< 2.5 μm) in the atmosphere.[22, 37, 38] Our study suggests that the particle size is a key factor affecting the core-shell mixing structure of OM and inorganic aerosols, in addition to O/C ratios and organic-to-inorganic ratios in the ambient air. Moreover, we found that the internally-mixed OM coatings and externally-mixed OM can have different effects on the particle

340 hygroscopic or CCN activities. Recently, Yu et al., (2019)[39] found that the absorption

341 cross section of the individual OM-coated particles significantly increased, when

342 assuming the OM coating consists of light-absorbing brown carbon.[39] We argue that

343 microscopic phase separation between organic and inorganic salts in fine aerosol

344 particles should be considered in modelling how the common phase separation

345 phenomenon in fine aerosol particles influences the regional climate, considering that

346 a large fraction of secondary organic aerosols is BrC in the North China Plain,[52] and

347 how SOM, as an important particle surface, influences heterogeneous reactions with

348 the reactive gases (e.g., N_2O_5 and VOCs)[16, 53, 54].

349

ASSOCIATED CONTENT

Supporting information

Detailed description of TEM images, NannoSIMS images, hygroscopic growth and data analysis (Table S1-S3 and Figure S1-S14)

AUTHOR INFORMATION

Corresponding authors

Weijun Li-Department of Atmospheric Sciences, School of Earth Sciences, Zhejiang University, 310027, Hangzhou, China

Zongbo Shi-School of Geography, Earth and Environmental Sciences, University of Birmingham, UK

Authors

Lei Liu-Department of Atmospheric Sciences, School of Earth Sciences, Zhejiang University, 310027, Hangzhou, China

Jian Zhang-Department of Atmospheric Sciences, School of Earth Sciences, Zhejiang University, 310027, Hangzhou, China

Liang Xu-Department of Atmospheric Sciences, School of Earth Sciences, Zhejiang University, 310027, Hangzhou, China

Yuanyuan Wang-Department of Atmospheric Sciences, School of Earth Sciences, Zhejiang University, 310027, Hangzhou, China

Yele Sun-State Key of Laboratory of Atmospheric Boundary Physics and Atmospheric Chemistry, Institute of Atmospheric Physics, Chinese Academy of Sciences, Beijing 100029, China

Notes

The authors declare no competing financial interest.

Acknowledgments

References

[1]   Wang, G.; Zhang, R.; Gomez, M. E.; Yang, L.; Levy Zamora, M.; Hu, M.; Lin, Y.; Peng, J.; Guo, S.; Meng, J.; Li, J.; Cheng, C.; Hu, T.; Ren, Y.; Wang, Y.; Gao, J.; Cao, J.; An, Z.; Zhou, W.; Li, G.; Wang, J.; Tian, P.; Marrero-Ortiz, W.; Secrest, J.; Du, Z.; Zheng, J.; Shang, D.; Zeng, L.; Shao, M.; Wang, W.; Huang, Y.; Wang, Y.; Zhu, Y.; Li, Y.; Hu, J.; Pan, B.; Cai, L.; Cheng, Y.; Ji, Y.; Zhang, F.; Rosenfeld, D.; Liss, P. S.; Duce, R. A.; Kolb, C. E.; Molina, M. J. Persistent sulfate formation from London Fog to Chinese haze. *P. Natl. Acad. Sci. USA.* **2016,** *113*, (48), 13630-13635.

[2]   Zheng, G. J.; Duan, F. K.; Su, H.; Ma, Y. L.; Cheng, Y.; Zheng, B.; Zhang, Q.; Huang, T.; Kimoto, T.; Chang, D.; Pöschl, U.; Cheng, Y. F.; He, K. B. Exploring the severe winter haze in Beijing: the impact of synoptic weather, regional transport and heterogeneous reactions. *Atmos. Chem. Phys.* **2015,** *15*, (6), 2969-2983.

[3]   Bianchi, F.; Tröstl, J.; Junninen, H.; Frege, C.; Henne, S.; Hoyle, C. R.; Molteni, U.; Herrmann, E.; Adamov, A.; Bukowiecki, N.; Chen, X.; Duplissy, J.; Gysel, M.; Hutterli, M.; Kangasluoma, J.; Kontkanen, J.; Kürten, A.; Manninen, H. E.; Münch, S.; Peräkylä, O.; Petäjä, T.; Rondo, L.; Williamson, C.; Weingartner, E.; Curtius, J.; Worsnop, D. R.; Kulmala, M.; Dommen, J.; Baltensperger, U. New particle formation in the free troposphere: A question of chemistry and timing. *Science.* **2016,** *352*, (6289), 1109-1112.

[4]   Riccobono, F.; Schobesberger, S.; Scott, C. E.; Dommen, J.; Ortega, I. K.; Rondo, L.; Almeida, J.; Amorim, A.; Bianchi, F.; Breitenlechner, M.; David, A.; Downard, A.; Dunne, E. M.; Duplissy, J.; Ehrhart, S.; Flagan, R. C.; Franchin, A.; Hansel, A.; Junninen, H.; Kajos, M.; Keskinen, H.; Kupc, A.; Kürten, A.; Kvashin, A. N.; Laaksonen, A.; Lehtipalo, K.; Makhmutov, V.; Mathot, S.; Nieminen, T.; Onnela, A.; Petäjä, T.; Praplan, A. P.; Santos, F. D.; Schallhart, S.; Seinfeld, J. H.; Sipilä, M.; Spracklen, D. V.;

402   Stozhkov, Y.; Stratmann, F.; Tomé, A.; Tsagkogeorgas, G.; Vaattovaara, P.; Viisanen, Y.; Vrtala, A.;

403   Wagner, P. E.; Weingartner, E.; Wex, H.; Wimmer, D.; Carslaw, K. S.; Curtius, J.; Donahue, N. M.; Kirkby,

404   J.; Kulmala, M.; Worsnop, D. R.; Baltensperger, U. Oxidation Products of Biogenic Emissions Contribute

405   to Nucleation of Atmospheric Particles. *Science.* **2014,** *344*, (6185), 717-721.

406   [5]   Yao, L.; Garmash, O.; Bianchi, F.; Zheng, J.; Yan, C.; Kontkanen, J.; Junninen, H.; Mazon, S. B.;

407   Ehn, M.; Paasonen, P.; Sipilä, M.; Wang, M.; Wang, X.; Xiao, S.; Chen, H.; Lu, Y.; Zhang, B.; Wang, D.;

408   Fu, Q.; Geng, F.; Li, L.; Wang, H.; Qiao, L.; Yang, X.; Chen, J.; Kerminen, V.-M.; Petäjä, T.; Worsnop,

409   D. R.; Kulmala, M.; Wang, L. Atmospheric new particle formation from sulfuric acid and amines in a

410   Chinese megacity. *Science.* **2018,** *361*, (6399), 278-281.

411   [6]   Guo, S.; Hu, M.; Zamora, M. L.; Peng, J.; Shang, D.; Zheng, J.; Du, Z.; Wu, Z.; Shao, M.; Zeng, L.;

412   Molina, M. J.; Zhang, R. Elucidating severe urban haze formation in China. *P. Natl. Acad. Sci. USA.*

413   **2014,** *111*, (49), 17373-17378.

414   [7]   Li, W.; Sun, J.; Xu, L.; Shi, Z.; Riemer, N.; Sun, Y.; Fu, P.; Zhang, J.; Lin, Y.; Wang, X.; Shao, L.;

415   Chen, J.; Zhang, X.; Wang, Z.; Wang, W. A conceptual framework for mixing structures in individual

416   aerosol particles. *J. Geophys. Res.* **2016,** *121*, (22), 13,784-13,798.

417   [8]   Jimenez, J. L.; Canagaratna, M. R.; Donahue, N. M.; Prevot, A. S. H.; Zhang, Q.; Kroll, J. H.;

418   DeCarlo, P. F.; Allan, J. D.; Coe, H.; Ng, N. L.; Aiken, A. C.; Docherty, K. S.; Ulbrich, I. M.; Grieshop,

419   A. P.; Robinson, A. L.; Duplissy, J.; Smith, J. D.; Wilson, K. R.; Lanz, V. A.; Hueglin, C.; Sun, Y. L.;

420   Tian, J.; Laaksonen, A.; Raatikainen, T.; Rautiainen, J.; Vaattovaara, P.; Ehn, M.; Kulmala, M.; Tomlinson,

421   J. M.; Collins, D. R.; Cubison, M. J.; E.; Dunlea, J.; Huffman, J. A.; Onasch, T. B.; Alfarra, M. R.;

422   Williams, P. I.; Bower, K.; Kondo, Y.; Schneider, J.; Drewnick, F.; Borrmann, S.; Weimer, S.; Demerjian,

423   K.; Salcedo, D.; Cottrell, L.; Griffin, R.; Takami, A.; Miyoshi, T.; Hatakeyama, S.; Shimono, A.; Sun, J.

Y.; Zhang, Y. M.; Dzepina, K.; Kimmel, J. R.; Sueper, D.; Jayne, J. T.; Herndon, S. C.; Trimborn, A. M.;

Williams, L. R.; Wood, E. C.; Middlebrook, A. M.; Kolb, C. E.; Baltensperger, U.; Worsnop, D. R.

Evolution of Organic Aerosols in the Atmosphere. *Science.* **2009,** *326*, (5959), 1525-1529.

[9]   Mikhailov, E.; Vlasenko, S.; Martin, S. T.; Koop, T.; Poschl, U. Amorphous and crystalline aerosol

particles interacting with water vapor: conceptual framework and experimental evidence for restructuring,

phase transitions and kinetic limitations. *Atmos. Chem. Phys.* **2009,** *9*, (24), 9491-9522.

[10] Knopf, D. A.; Wang, B.; Laskin, A.; Moffet, R. C.; Gilles, M. K. Heterogeneous nucleation of ice

on anthropogenic organic particles collected in Mexico City. *Geophy. Res. Lett.* **2010,** *37*, (11), L11803.

[11] Dusek, U.; Frank, G. P.; Curtius, J.; Drewnick, F.; Schneider, J.; Kurten, A.; Rose, D.; Andreae, M.

O.; Borrmann, S.; Poschl, U. Enhanced organic mass fraction and decreased hygroscopicity of cloud

condensation nuclei (CCN) during new particle formation events. *Geophy. Res. Lett.* **2010,** *37*, L03804.

[12] Bertram, A. K.; Martin, S. T.; Hanna, S. J.; Smith, M. L.; Bodsworth, A.; Chen, Q.; Kuwata, M.;

Liu, A.; You, Y.; Zorn, S. R. Predicting the relative humidities of liquid-liquid phase separation,

efflorescence, and deliquescence of mixed particles of ammonium sulfate, organic material, and water

using the organic-to-sulfate mass ratio of the particle and the oxygen-to-carbon elemental ratio of the

organic component. *Atmos. Chem. Phys.* **2011,** *11*, (21), 10995-11006.

[13] Sareen, N.; Schwier, A. N.; Lathem, T. L.; Nenes, A.; McNeill, V. F. Surfactants from the gas phase

may promote cloud droplet formation. *P. Natl. Acad. Sci. USA.* **2013,** *110*, (8), 2723-2728.

[14] Shrivastava, M.; Lou, S.; Zelenyuk, A.; Easter, R. C.; Corley, R. A.; Thrall, B. D.; Rasch, P. J.; Fast,

J. D.; Massey Simonich, S. L.; Shen, H.; Tao, S. Global long-range transport and lung cancer risk from

polycyclic aromatic hydrocarbons shielded by coatings of organic aerosol. *P. Natl. Acad. Sci. USA.* **2017,**

114, (6), 1246-1251.

446 [15] Mu, Q.; Shiraiwa, M.; Octaviani, M.; Ma, N.; Ding, A.; Su, H.; Lammel, G.; Pöschl, U.; Cheng, Y.

447 Temperature effect on phase state and reactivity controls atmospheric multiphase chemistry and transport

448 of PAHs. *Sci. Adv.* **2018**, *4*, (3), eaap7314, 1-8.

449 [16] Zhang, Y.; Chen, Y.; Lambe, A. T.; Olson, N. E.; Lei, Z.; Craig, R. L.; Zhang, Z.; Gold, A.; Onasch,

450 T. B.; Jayne, J. T.; Worsnop, D. R.; Gaston, C. J.; Thornton, J. A.; Vizuete, W.; Ault, A. P.; Surratt, J. D.

451 Effect of the Aerosol-Phase State on Secondary Organic Aerosol Formation from the Reactive Uptake of

452 Isoprene-Derived Epoxydiols (IEPOX). *Environ. Sci. Techn. Lett.* **2018**, *5*, (3), 167-174.

453 [17] You, Y.; Renbaum-Wolff, L.; Carreras-Sospedra, M.; Hanna, S. J.; Hiranuma, N.; Kamal, S.; Smith,

454 M. L.; Zhang, X.; Weber, R. J.; Shilling, J. E.; Dabdub, D.; Martin, S. T.; Bertram, A. K. Images reveal

455 that atmospheric particles can undergo liquid–liquid phase separations. *P. Natl. Acad. Sci. USA.* **2012,**

456 *109*, (33), 13188-13193.

457 [18] Li, W. J.; Shao, L. Y. Mixing and water-soluble characteristics of particulate organic compounds in

458 individual urban aerosol particles. *J. Geophys. Res.* **2010**, *115*, D02301, doi:10.1029/2009JD012575.

459 [19] Moffet, R. C.; Henn, T. R.; Tivanski, A. V.; Hopkins, R. J.; Desyaterik, Y.; Kilcoyne, A. L. D.;

460 Tyliszczak, T.; Fast, J.; Barnard, J.; Shutthanandan, V.; Cliff, S. S.; Perry, K. D.; Laskin, A.; Gilles, M.

461 K. Microscopic characterization of carbonaceous aerosol particle aging in the outflow from Mexico City.

462 *Atmos. Chem. Phys.* **2010**, *10*, (3), 961-976.

463 [20] Li, W.; Shao, L.; Zhang, D.; Ro, C.-U.; Hu, M.; Bi, X.; Geng, H.; Matsuki, A.; Niu, H.; Chen, J. A

464 review of single aerosol particle studies in the atmosphere of East Asia: morphology, mixing state, source,

465 and heterogeneous reactions. *J. Clean. Prod.* **2016,** *112, Part 2*, 1330-1349.

466 [21] Adachi, K.; Buseck, P. R. Internally mixed soot, sulfates, and organic matter in aerosol particles

467 from Mexico City. *Atmos. Chem. Phys.* **2008**, *8*, (21), 6469-6481.

468   [22] Russell, L. M.; Maria, S. F.; Myneni, S. C. B. Mapping organic coatings on atmospheric particles.

469   *Geophy. Res. Lett.* **2002,** *29*, (16), 1-4.

470   [23] Tervahattu, H.; Juhanoja, J.; Kupiainen, K. Identification of an organic coating on marine aerosol

471   particles by TOF-SIMS. *J. Geophy. Res.* **2002,** *107*, (D16), 4319.

472   [24] Shiraiwa, M.; Ammann, M.; Koop, T.; Pöschl, U. Gas uptake and chemical aging of semisolid

473   organic aerosol particles. *P. Natl. Acad. Sci. USA.* **2011,** *108*, (27), 11003-11008.

474   [25] Riva, M.; Bell, D. M.; Hansen, A.-M. K.; Drozd, G. T.; Zhang, Z.; Gold, A.; Imre, D.; Surratt, J. D.;

475   Glasius, M.; Zelenyuk, A. Effect of Organic Coatings, Humidity and Aerosol Acidity on Multiphase

476   Chemistry of Isoprene Epoxydiols. *Environ. Sci. Techn.* **2016,** *50*, (11), 5580-5588.

477   [26] Kanakidou, M.; Seinfeld, J. H.; Pandis, S. N.; Barnes, I.; Dentener, F. J.; Facchini, M. C.; Van

478   Dingenen, R.; Ervens, B.; Nenes, A.; Nielsen, C. J.; Swietlicki, E.; Putaud, J. P.; Balkanski, Y.; Fuzzi, S.;

479   Horth, J.; Moortgat, G. K.; Winterhalter, R.; Myhre, C. E. L.; Tsigaridis, K.; Vignati, E.; Stephanou, E.

480   G.; Wilson, J. Organic aerosol and global climate modelling: a review. *Atmos. Chem. Phys.* **2005,** *5*,

481   1053-1123.

482   [27] Song, M.; Marcolli, C.; Krieger, U. K.; Lienhard, D. M.; Peter, T. Morphologies of mixed

483   organic/inorganic/aqueous aerosol droplets. *Faraday Discuss.* **2013,** *165*, (0), 289-316.

484   [28] O'Brien, R. E.; Wang, B.; Kelly, S. T.; Lundt, N.; You, Y.; Bertram, A. K.; Leone, S. R.; Laskin, A.;

485   Gilles, M. K. Liquid–Liquid Phase Separation in Aerosol Particles: Imaging at the Nanometer Scale.

486   *Environ. Sci. Techn.* **2015,** *49*, (8), 4995-5002.

487   [29] Veghte, D. P.; Altaf, M. B.; Freedman, M. A. Size Dependence of the Structure of Organic Aerosol.

488   *J. Am. Chem. Soc.* **2013,** *135*, (43), 16046-16049.

489   [30] Altaf, M. B.; Freedman, M. A. Effect of Drying Rate on Aerosol Particle Morphology. *J. Phys.*

Chem. Lett. **2017,** *8*, (15), 3613-3618.

[31] Cheng, Y.; Su, H.; Koop, T.; Mikhailov, E.; Pöschl, U. Size dependence of phase transitions in aerosol nanoparticles. *Nat. Commun.* **2015,** *6*, 5923-5930.

[32] Sun, J.; Liu, L.; Xu, L.; Wang, Y.; Wu, Z.; Hu, M.; Shi, Z.; Li, Y.; Zhang, X.; Chen, J.; Li, W. Key Role of Nitrate in Phase Transitions of Urban Particles: Implications of Important Reactive Surfaces for Secondary Aerosol Formation. *J. Geophy. Res.* **2018,** *123*, (2), 1234-1243.

[33] Song, M.; Marcolli, C.; Krieger, U. K.; Zuend, A.; Peter, T. Liquid-liquid phase separation in aerosol particles: Dependence on O:C, organic functionalities, and compositional complexity. *Geophy. Res. Lett.* **2012,** *39*, (19), L19801.

[34] Zhang, Y.; Chen, Y.; Lei, Z.; Olson, N. E.; Riva, M.; Koss, A. R.; Zhang, Z.; Gold, A.; Jayne, J. T.; Worsnop, D. R.; Onasch, T. B.; Kroll, J. H.; Turpin, B. J.; Ault, A. P.; Surratt, J. D. Joint Impacts of Acidity and Viscosity on the Formation of Secondary Organic Aerosol from Isoprene Epoxydiols (IEPOX) in Phase Separated Particles. *ACS Earth and Space Chem.* **2019,** *3*, (12), 2646-2658.

[35] Olson, N. E.; Lei, Z.; Craig, R. L.; Zhang, Y.; Chen, Y.; Lambe, A. T.; Zhang, Z.; Gold, A.; Surratt, J. D.; Ault, A. P. Reactive Uptake of Isoprene Epoxydiols Increases the Viscosity of the Core of Phase-Separated Aerosol Particles. *ACS Earth and Space Chem.* **2019,** *3*, (8), 1402-1414.

[36] Riemer, N.; Ault, A. P.; West, M.; Craig, R. L.; Curtis, J. H. Aerosol Mixing State: Measurements, Modeling, and Impacts. *Rev. Geophys.* **2019,** *57*, https://doi.org/10.1029/2018RG000615.

[37] Pöhlker, C.; Wiedemann, K. T.; Sinha, B.; Shiraiwa, M.; Gunthe, S. S.; Smith, M.; Su, H.; Artaxo, P.; Chen, Q.; Cheng, Y.; Elbert, W.; Gilles, M. K.; Kilcoyne, A. L. D.; Moffet, R. C.; Weigand, M.; Martin, S. T.; Pöschl, U.; Andreae, M. O. Biogenic potassium salt particles as seeds for secondary organic aerosol in the Amazon. *Science.* **2012,** *337*, (6098), 1075-1078.

512   [38] Takahama, S.; Liu, S.; Russell, L. M. Coatings and clusters of carboxylic acids in carbon-containing

513   atmospheric particles from spectromicroscopy and their implications for cloud-nucleating and optical

514   properties. *J. Geophys. Res.* **2010,** *115*, D01202, doi:10.1029/2009JD012622.

515   [39] Yu, H.; Li, W.; Zhang, Y.; Tunved, P.; Dall'Osto, M.; Shen, X.; Sun, J.; Zhang, X.; Zhang, J.; Shi,

516   Z. Organic coating on sulfate and soot particles during late summer in the Svalbard Archipelago. *Atmos.*

517   *Chem. Phys.* **2019,** *19*, (15), 10433-10446.

518   [40] Sun, Y.; Jiang, Q.; Xu, Y.; Ma, Y.; Zhang, Y.; Liu, X.; Li, W.; Wang, F.; Li, J.; Wang, P.; Li, Z.

519   Aerosol Characterization over the North China Plain: Haze Life Cycle and Biomass Burning Impacts in

520   Summer. *J. Geophy. Res.* **2016,** *121*, (5), 2508-2521.

521   [41] Zhang S J, X. L., GUO X M, HUANG D, LI W J Influence of Secondary Organic Coating on

522   Hygroscopicity of Sodium Chloride Core: Based on Mircro-scale Single Particle Analysis. *Environ. Sci.*

523   **2020,** *41*, (5), 21-29 (In Chinese).

524   [42] Li, W.; Xu, L.; Liu, X.; Zhang, J.; Lin, Y.; Yao, X.; Gao, H.; Zhang, D.; Chen, J.; Wang, W.; Harrison,

525   R. M.; Zhang, X.; Shao, L.; Fu, P.; Nenes, A.; Shi, Z. Air pollution–aerosol interactions produce more

526   bioavailable iron for ocean ecosystems. *Sci. Adv.* **2017,** *3*, (3), e1601749, 1-6.

527   [43] Petters, M. D.; Kreidenweis, S. M. A single parameter representation of hygroscopic growth and

528   cloud condensation nucleus activity. *Atmos. Chem. Phys.* **2007,** *7*, (8), 1961-1971.

529   [44] Hu, W. W.; Hu, M.; Yuan, B.; Jimenez, J. L.; Tang, Q.; Peng, J. F.; Hu, W.; Shao, M.; Wang, M.;

530   Zeng, L. M.; Wu, Y. S.; Gong, Z. H.; Huang, X. F.; He, L. Y. Insights on organic aerosol aging and the

531   influence of coal combustion at a regional receptor site of central eastern China. *Atmos. Chem. Phys.*

532   **2013,** *13*, (19), 10095-10112.

533   [45] Xu, W. Q.; Sun, Y. L.; Chen, C.; Du, W.; Han, T. T.; Wang, Q. Q.; Fu, P. Q.; Wang, Z. F.; Zhao, X.

J.; Zhou, L. B.; Ji, D. S.; Wang, P. C.; Worsnop, D. R. Aerosol composition, oxidation properties, and sources in Beijing: results from the 2014 Asia-Pacific Economic Cooperation summit study. *Atmos. Chem. Phys.* **2015,** *15*, (23), 13681-13698.

[46] Ott, E.-J. E.; Tackman, E. C.; Freedman, M. A. Effects of Sucrose on Phase Transitions of Organic/Inorganic Aerosols. *ACS Earth and Space Chem.* **2020,** *4*, (4), 591-601.

[47] Stewart, D. J.; Cai, C.; Nayler, J.; Preston, T. C.; Reid, J. P.; Krieger, U. K.; Marcolli, C.; Zhang, Y. H. Liquid–Liquid Phase Separation in Mixed Organic/Inorganic Single Aqueous Aerosol Droplets. *J. Phys. Chem. A.* **2015,** *119*, (18), 4177-4190.

[48] Kucinski, T. M.; Dawson, J. N.; Freedman, M. A. Size-Dependent Liquid–Liquid Phase Separation in Atmospherically Relevant Complex Systems. *J. Phys. Chem. Lett.* **2019,** *10*, (21), 6915-6920.

[49] Brooks, S. D.; Wise, M. E.; Cushing, M.; Tolbert, M. A. Deliquescence behavior of organic/ammonium sulfate aerosol. *Geophy. Res. Lett.* **2002,** *29*, (19), 1917-1921.

[50] Davies, J. F.; Miles, R. E. H.; Haddrell, A. E.; Reid, J. P. Influence of organic films on the evaporation and condensation of water in aerosol. *P. Natl. Acad. Sci. USA.* **2013,** *110*, (22), 8807-8812.

[51] Gunthe, S. S.; Rose, D.; Su, H.; Garland, R. M.; Achtert, P.; Nowak, A.; Wiedensohler, A.; Kuwata, M.; Takegawa, N.; Kondo, Y.; Hu, M.; Shao, M.; Zhu, T.; Andreae, M. O.; Pöschl, U. Cloud condensation nuclei (CCN) from fresh and aged air pollution in the megacity region of Beijing. *Atmos. Chem. Phys.* **2011,** *11*, (21), 11023-11039.

[52] Wang, L.; Wang, X.; Gu, R.; Wang, H.; Yao, L.; Wen, L.; Zhu, F.; Wang, W.; Xue, L.; Yang, L.; Lu, K.; Chen, J.; Wang, T.; Zhang, Y.; Wang, W. Observations of fine particulate nitrated phenols in four sites in northern China: concentrations, source apportionment, and secondary formation. *Atmos. Chem. Phys.* **2018,** *18*, (6), 4349-4359.

556   [53] Gaston, C. J.; Thornton, J. A.; Ng, N. L. Reactive uptake of N2O5 to internally mixed inorganic and

557   organic particles: the role of organic carbon oxidation state and inferred organic phase separations. *Atmos.*

558   *Chem. Phys.* **2014,** *14*, (11), 5693-5707.

559   [54] McNeill, V. F.; Patterson, J.; Wolfe, G. M.; Thornton, J. A. The effect of varying levels of surfactant

560   on the reactive uptake of N2O5 to aqueous aerosol. *Atmos. Chem. Phys.* **2006,** *6*, (6), 1635-1644.

561
562

563 **Abstract Graph**

564

565

566
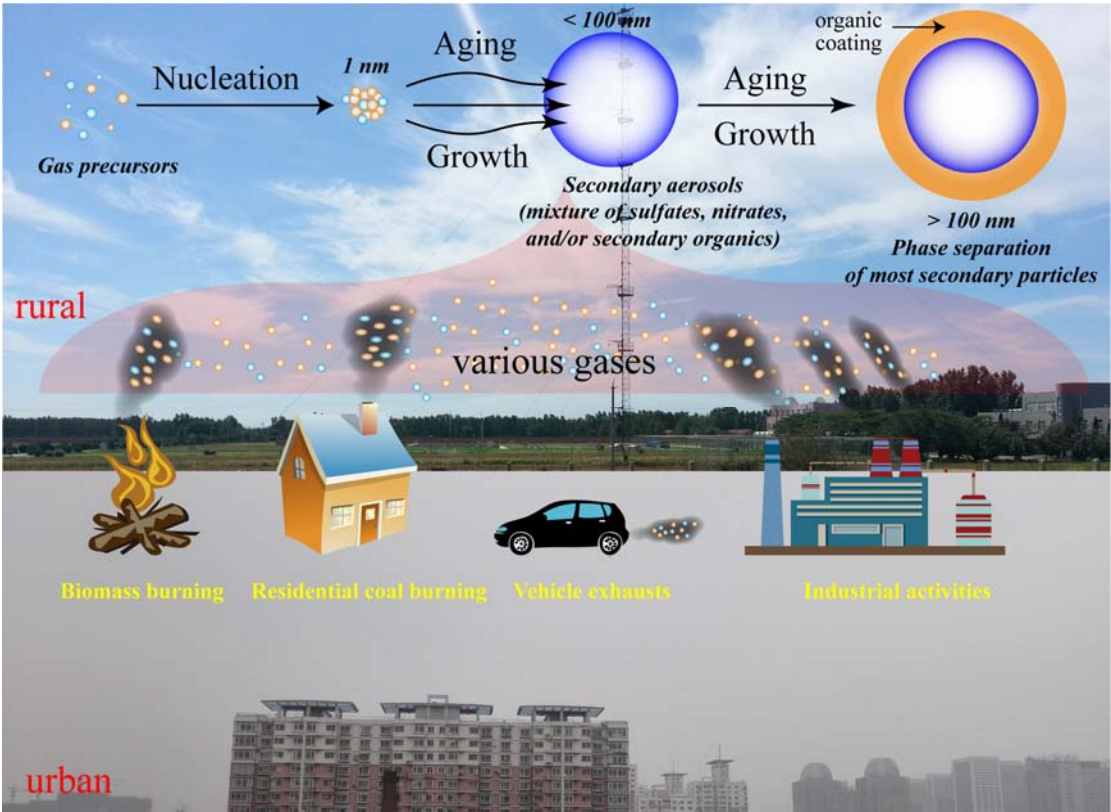
Figure Captions:
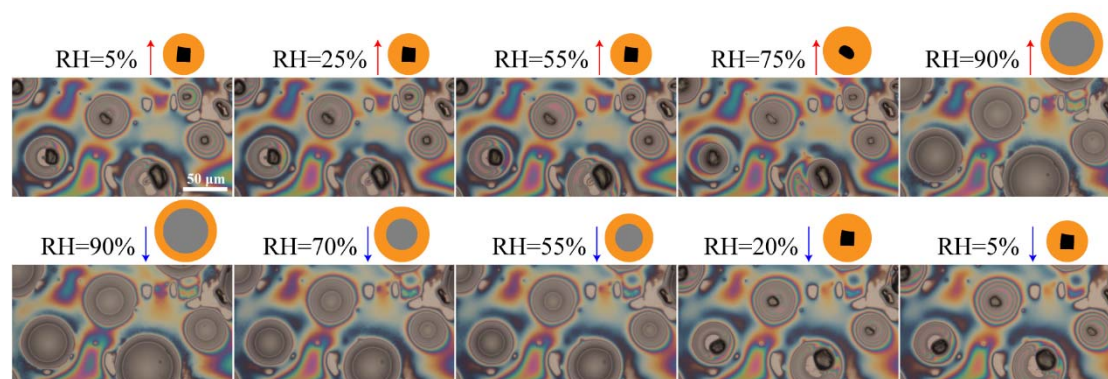
Figure 1 Phase separation at different RH in surrogate particles prepared in laboratory. Continuous phase separation in individual particles containing NaCl core (dark color) and secondary organic coating from high to low RH. Red arrow indicates the hydration (↑) and dehydration (↓) process of particles following the RH.
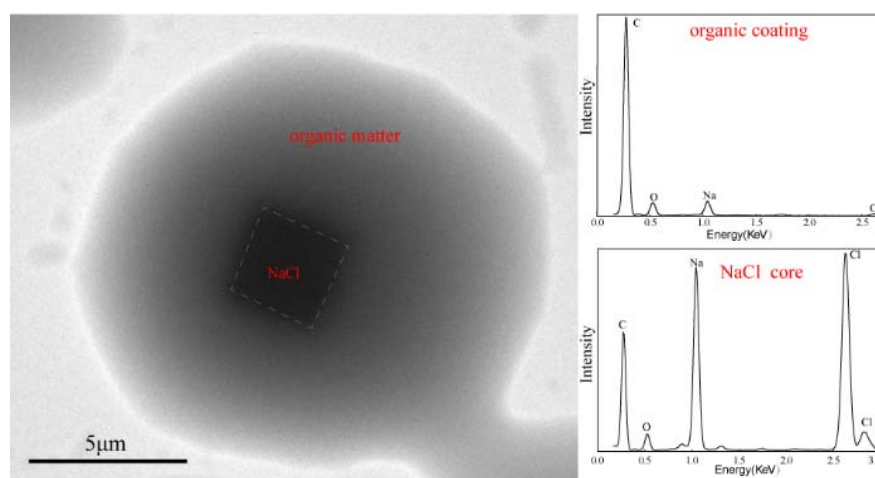

Figure 2 Morphology and composition of an individual particle showing phase separation between NaCl and organic coating. The sample observed in TEM is same to Figure 1.
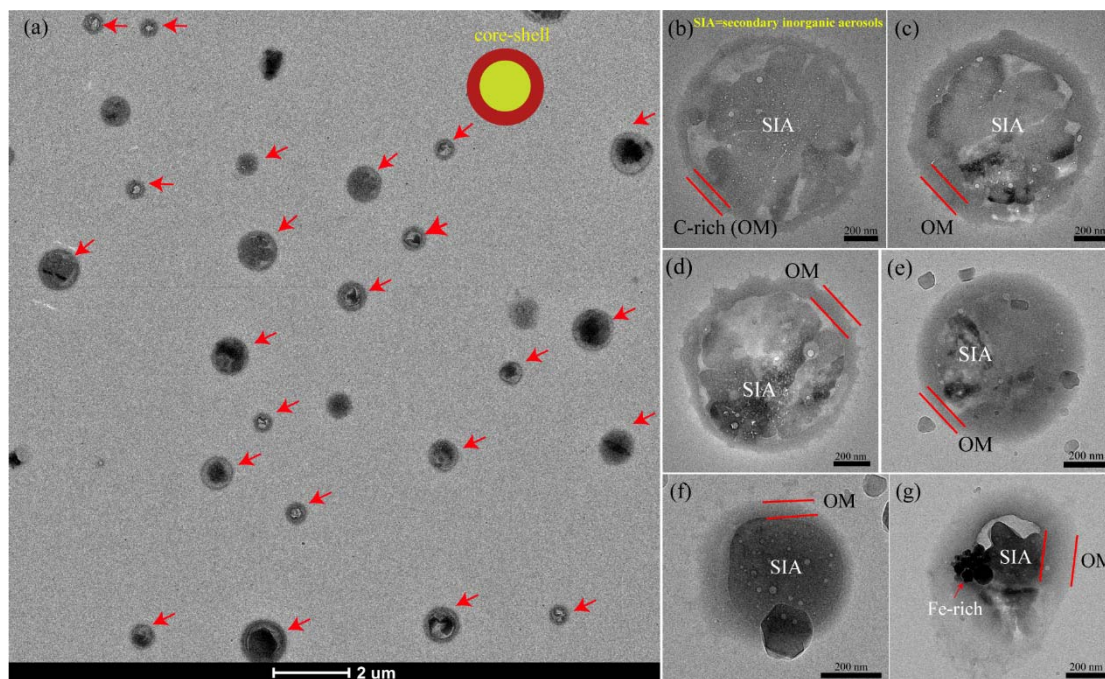
Figure 3. Cryo-TEM images showing internally mixed secondary inorganic aerosols and organic matter (OM) in individual particles with minimum damage under the electron beam. (a) Low magnification cryo-TEM image showing particles containing OM coating and inorganic cores collected at rural site. Red arrows show the core-shell structure particles. (f-g) High magnification cryo-TEM images showing secondary inorganic aerosols (SIA) with different size coated by different thickness of OM. Red line indicates OM coating.
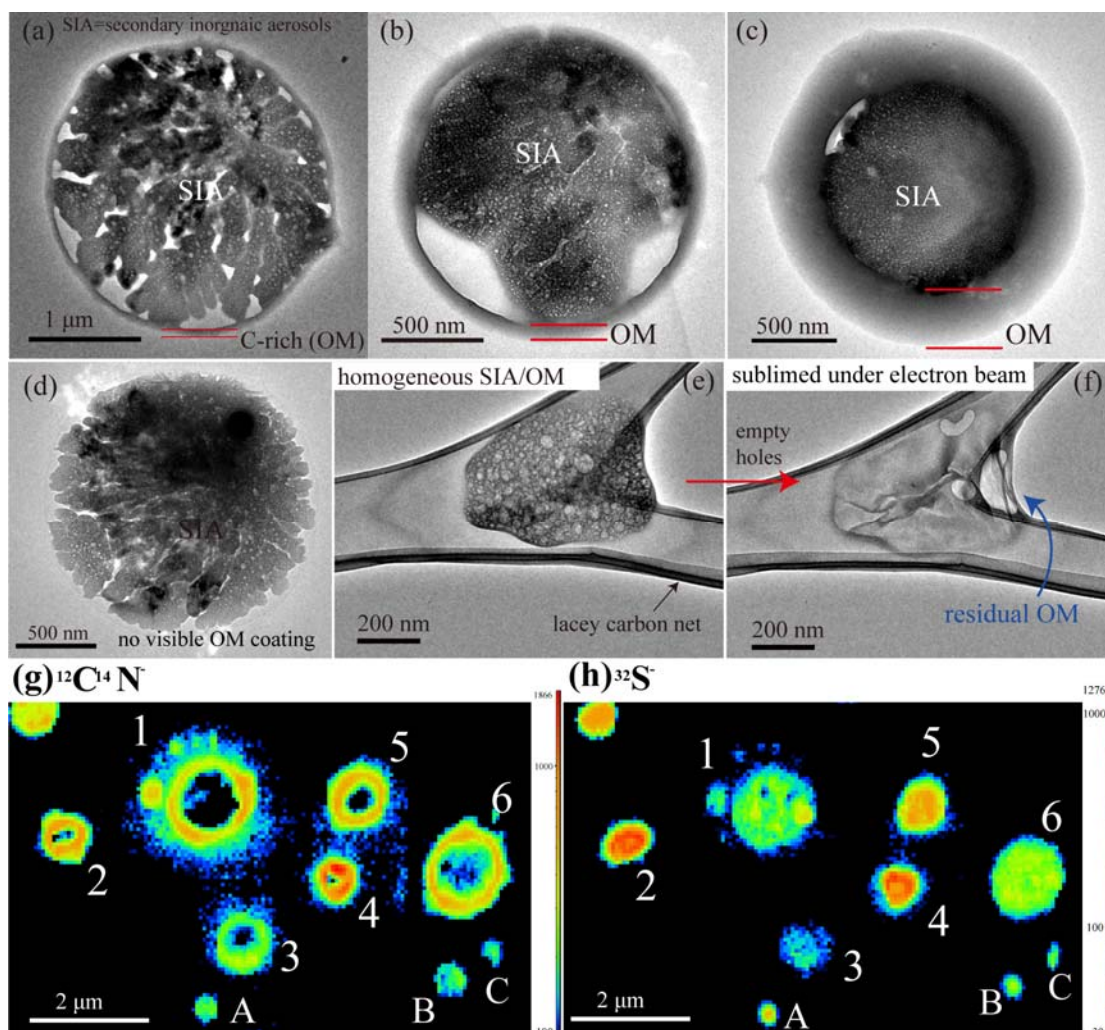
Figure 4. TEM images and NanoSIMS ion intensity threshold maps of individual particles collected at the rural site. (a-c) Sulfate particle coated by different thickness of OM. Red line indicates OM coating. (d) No visible OM coating on sulfate particle. (e-f) The ultrafine SIA particle under the electron beam and its corresponding sublimed particle, which contains residual OM. (g) $^{12}C^{14}N^-$ ion intensity map showing OM distribution in individual particles. (h) $^{32}S^-$ ion intensity map showing sulfate distribution in individual particles. The number 1-6 represents the OM-coating structure and the letter A-C represents homogeneous structure. All the particle images were taken in room temperature (20 °C) and vacuum condition. $^{12}C^-$ and $^{12}C^{14}N^-$ ion intensity maps were compared in supplemental materials.
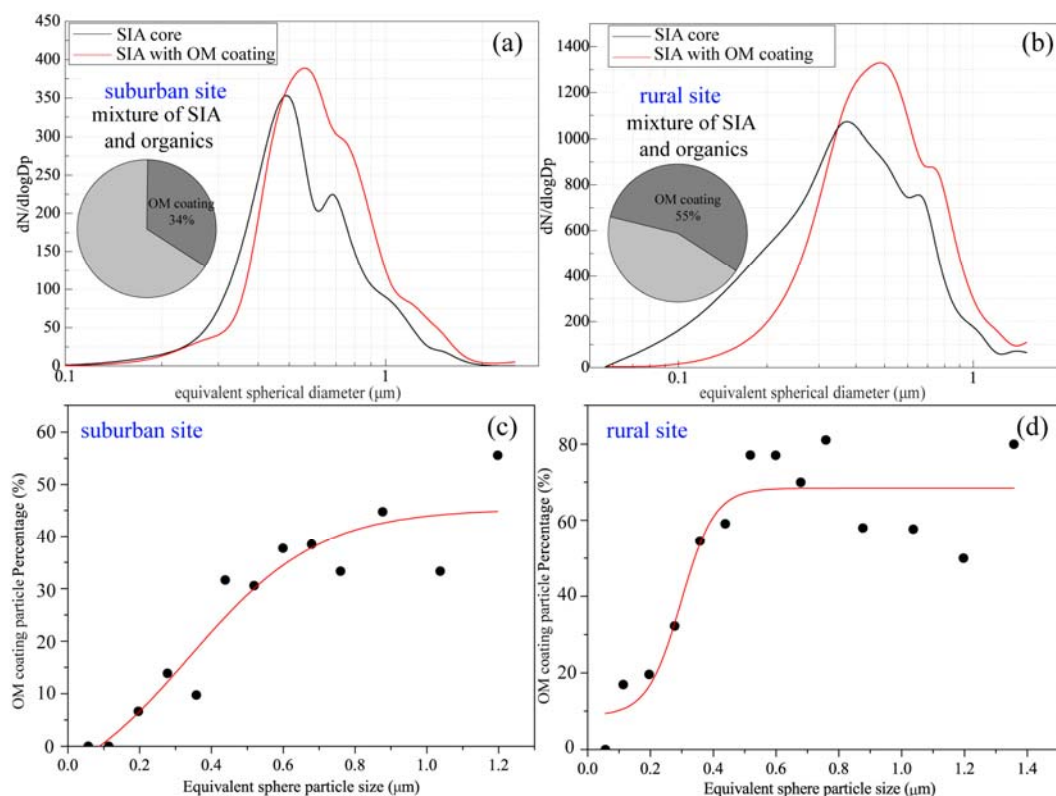
Figure 5. Percentages of inorganic particles with and without OM coating and size distributions of OM-coating particles and their inorgnaic core. 433 particles at suburban Xianghe site and 1117 at rural Yucheng site were analyzed, respectively. (a) Two main peaks at 480 nm for inorganic particle without OM coating and 560 nm for inorganic particle with OM coating at Xianghe site. (b) The main peak at 370 nm for inorganic particle without OM coating and 490 nm for inorganic particle with OM coating at Yucheng site. (c-d) Variation in percentage of OM-coating particles in all S-rich particles with size. ECD of individual particles converted to ESD based on supplemental materials.